J Sol-Gel Sci Technol (2009) 49:71–77
DOI 10.1007/s10971-008-1829-6

ORIGINAL PAPER

Synthesis of silica xerogels with highly distinct morphologies in the presence of imidazolium ionic liquids

R. K. Donato · M. V. Migliorini · M. A. Benvegnú · M. P. Stracke · M. A. Gelesky · F. A. Pavan · C. M. L. Schrekker · E. V. Benvenutti · J. Dupont · H. S. Schrekker

Received: 5 June 2008 / Accepted: 20 August 2008 / Published online: 2 September 2008

Abstract This article describes the preparation of silica xerogels by the sol–gel technique, using tetraethoxysilane as precursor and hydrofluoric acid as catalyst, in the presence of imidazolium ionic liquids (ILs). The applied ILs **1–3** contained the 1-monoethylene glycol monomethyl ether-3-methylimidazolium cation in combination with the methanesulfonate (**1**), tetrafluoroborate (**2**) and hexafluorophosphate (**3**) anions, respectively. Characterization of these materials was performed by photography, scanning electron microscopy, atomic force microscopy, X-ray diffraction, thermogravimetric analysis and nitrogen adsorption-desorption isotherms. The IL anion was identified as a powerful morphology controller. The methanesulfonate anion of IL **1** induced the formation of a compact lamellar monolith with an interlamellar distance of 1.5 nm and a flat surface. A free flowing powder of aggregated spherical particles was obtained in the presence of tetrafluoroborate IL **2**, and the hexafluorophosphate anion of IL **3** induced the formation of porcelain like aggregates with honeycomb shapes.

Keywords Imidazolium ionic liquid · Silica xerogel · Morphology · Sol–gel · Anion

Electronic supplementary material The online version of this article (doi:10.1007/s10971-008-1829-6) contains supplementary material, which is available to authorized users.

R. K. Donato · M. V. Migliorini · M. A. Benvegnú · H. S. Schrekker (✉)
Laboratory of Technological Processes and Catalysis, Institute of Chemistry, Universidade Federal do Rio Grande do Sul, Av. Bento Gonçalves 9500, P.O. Box 15003, CEP: 91501-970 Porto Alegre, RS, Brazil
e-mail: schrekker@iq.ufrgs.br

M. P. Stracke · M. A. Gelesky · F. A. Pavan · C. M. L. Schrekker · J. Dupont
Laboratory of Molecular Catalysis, Institute of Chemistry, Universidade Federal do Rio Grande do Sul, Av. Bento Gonçalves 9500, P.O. Box 15003, CEP: 91501-970 Porto Alegre, RS, Brazil

F. A. Pavan
Universidade Federal do Pampa, Rua Carlos Barbosa s/n, Getúlio Vargas, CEP: 96412-420 Bage, RS, Brazil

E. V. Benvenutti
Laboratory of Solid State Chemistry and Surfaces, Institute of Chemistry, Universidade Federal do Rio Grande do Sul, Av. Bento Gonçalves 9500, P.O. Box 15003, CEP: 91501-970 Porto Alegre, RS, Brazil

1 Introduction

Ionic liquids (ILs), salts that are liquid below 100 °C, typically comprise of a large organic cation together with an organic or inorganic anion [1, 2]. The class of imidazolium cation based ILs has proven to be highly attractive and versatile. Frequently encountered favorable characteristics of imidazolium ILs are for instance high thermal stability, being liquid over a wide temperature range, air and moisture stability, very low vapor pressure, wide electrochemical window, high conductivity and ionic mobility, easy recycling, and being a good solvent for a wide variety of organic and inorganic chemical compounds. Besides, imidazolium ILs are "designable" as structural modifications in both the cation (especially the 1 and 3 positions of the imidazolium ring) and anion permit the tuning of properties like, e.g., miscibility with water and organic solvents, melting point and viscosity. As a result, applications of imidazolium ILs are numerous and found in the fields of extraction and separation processes [3], synthetic chemistry [2], catalysis (organometallic [2, 4]/transition-metal nanoparticle [5, 6]/bio [7]) and electrochemistry [8].

Imidazolium ILs exist as hydrogen-bonded networks in both solid and liquid phases [9]. Each imidazolium cation is surrounded by anions and each anion is surrounded by imidazolium cations in an extended network due to the formation of hydrogen bonds between the imidazolium ring protons and anions. This induces structural directionality and, as a consequence, imidazolium ILs exist as pre-organized structures. It is especially this feature what distinguishes the imidazolium ILs from other types of ILs that form neutral ion pairs. These imidazolium IL structures can adapt their organization to the properties of many species as they contain hydrophobic and hydrophilic regions, and a high directional polarizability [10, 11]. This structural organization of ILs can be used as "entropic driver" for spontaneous, well-defined and extended ordering of nano-scale structures. Indeed, the unique combination of adaptability towards other molecules and phases associated to the strong hydrogen-bond-driven structure makes ILs potential key tools in the preparation of a new generation of chemical nanostructures [12, 13]. As a consequence, imidazolium ILs have a huge potential for applications in the field of materials science [14]. Imidazolium ILs provided new strategies for the preparation of metal nanoparticles with small diameter and narrow size distribution [5, 6]. Furthermore, imidazolium ILs are excellent "templates" for the preparation of nanoporous inorganic materials like, e.g., silica and titanium oxide, by the sol–gel process [14, 15].

Unique silica xerogels and aerogels have been synthesized by the sol–gel process with ILs, including highly organized nanostructures [16]. Furthermore, this technology furnished access to materials with large specific surface areas, high porosities and controllable pore sizes with a narrow size distribution [14]. These silicas have found application as, for instance, catalyst, catalyst support, chromatographic material, immobilizer, optics and electronics, and "template" for the formation of advanced nanostructures. However, these studies were almost exclusively performed with the class of 1-alkyl-3-methylimidazolium ILs and halogen counter-ions. Lately, we reported about the preparation and characterization of ether-functionalized imidazolium ILs [17–20]. Gold(0) nanoparticles were successfully prepared in the 1-triethylene glycol monomethyl ether-3-methylimidazolium methanesulfonate IL, which allowed studying the coordination and stabilization mode of the imidazolium cation by surface-enhanced Raman spectroscopy [21]. In this study, three ether-functionalized imidazolium ILs (Fig. 1) were applied in the preparation of silica xerogels by the sol–gel technique. These 1-monoethylene glycol monomethyl ether-3-methylimidazolium cation based ILs allowed to study the effect of the IL anion, which showed to play a predominant role as silica xerogels with highly distinct morphologies were obtained.

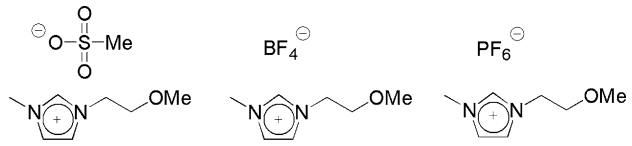

1 $[C_3O_1MIm][H_3CSO_3]$ **2** $[C_3O_1MIm][BF_4]$ **3** $[C_3O_1MIm][PF_6]$

Fig. 1 Imidazolium ionic liquids applied in this work

2 Experimental

2.1 Materials

The solvents acetone and ethanol were purchased from VETEC Química Fina LTDA and used without further purification. Tetraethoxysilane (TEOS) was used as purchased from Sigma-Aldrich and aqueous HF was used as purchased from SYNTH. Deionized water was used from Easy pure LF. $CDCl_3$ and D_2O were purchased from Cambridge Isotope Laboratories. A procedure reported previously in the literature was used for the synthesis of ILs **1–3** and the spectral data were in accordance with the literature data [17, 22, 23].

2.2 Silica xerogel

A modification of a literature procedure was used for the preparation of the silica xerogels [24]. TEOS (10 mL) was heated in a beaker to 60 °C. A solution of IL **1–3** (1.0 mL) in EtOH (5.0 mL) was added under stirring at 60 °C, followed by the HF catalyst (deionized water (2.0 mL) and aqueous HF (2.2×10^{-3} M, 0.5 mL)). The beaker was covered with a watch glass and the reaction mixture was stirred for 10 min at 60 °C. The reaction mixture was left at 60 °C without stirring, until dryness of the formed silica xerogels **S1–3** (between 24 and 48 h). Photographs were taken at this stage. The silicas **S1–3** were grinded into fine powders and dried under vacuum (5 h at 80 °C). TGA and SEM analysis were performed at this stage. Soxhlet extractions with acetone for 24 h were performed to remove the respective ILs. The extracted xerogels were dried under vacuum (5 h at 80 °C) and characterized by TGA, nitrogen adsorption-desorption isotherms, AFM, XRD and SEM. ^{1}H NMR analysis was performed to study the identity of the recovered ILs after acetone removal under vacuum.

2.3 Characterization

TGA measurements were performed on a TA Instruments Q50 thermogravimetric analyzer. The TGA instrument was calibrated using nickel. An average sample weight of 8–12 mg was placed in a platinum pan and heated at 20 °C/

min from ca. 30–800 °C under a flow of nitrogen. The silica xerogels were analyzed by SEM using a JEOL model JSM 5800 with 20 kV. A powder of each sample was placed on a sample holder covered with a carbon tab and metallized with gold during 2.5 min. under a cathodic atomizer blazer. Atomic force microscopy (AFM) images of silica surfaces were obtained using an Atomic Force Microscope, Nanoscope IIIa®, manufactured by Digital Instruments Co., using the contact mode technique with probes of silicon nitride. Samples were compressed in the form of tablets and fragments of roughly 16 mm^2 were employed for the analysis. WS M 4.0 software from Nanotec Electronic S.L. was used for the image treatments. The phase structures of silica xerogels were characterized by X-ray diffraction (XRD). Silica powders were placed in the sample holder. The XRD experiments were carried out on a SIEMENS D500 diffractometer equipped with a curved graphite crystal as monochromator using Cu Kα radiation ($\lambda = 1.5406$ Å). The diffraction data were collected at room temperature in a Bragg-Brentano θ–2θ geometry. The equipment was operated at 40 kV and 17.5 mA with a scan range between 1° and 45°. The diffractograms were obtained with a constant step, $\Delta 2\theta = 0.05°$. The N_2 adsorption-desorption isotherms of previously degassed silica xerogels (120 °C for 2 h) were determined at nitrogen boiling point temperature, using a homemade volumetric apparatus, connected to a turbo molecular Edwards vacuum line system. The pressure measurements were made employing a capillary Hg barometer and a Pirani gauge. The specific surface areas and the pore size distributions were determined using the BET (4-point evaluation) and BJH (performed on the desorption branch) methods, respectively. ^{1}H NMR spectra of the ILs were recorded on a Varian Inova 300 MHz spectrometer in $CDCl_3$ or D_2O.

3 Results and discussion

The three silica xerogels **S1–3** were prepared by the sol–gel technique (Scheme 1), using tetraethoxysilane as precursor and hydrofluoric acid as catalyst, in the presence of the imidazolium ILs **1–3**. The reactions were performed under identical conditions, which allowed to study the influence of the IL anions: methanesulfonate (IL **1**); tetrafluoroborate (IL **2**) and hexafluorophosphate (IL **3**), respectively (Fig. 1).

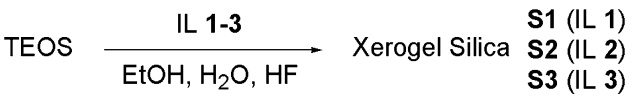

Scheme 1 Silica xerogels prepared in this work

These sol–gel reactions yielded 4.4 g (**S1**), 3.7 g (**S2**) and 3.3 g (**S3**), respectively. Fractions of same weight demonstrated large differences in occupied volumes, where **S1** showed the highest density and **S2** the lowest density. The reaction with IL **1** presented a gelation time of 24 h and ageing/drying time of 24 h. In contrast, the xerogels **S2** and **S3** showed a gelation time of 12 h and ageing/drying time of 12 h. Interestingly, these three xerogels were obtained with highly distinct visual appearances. The different gelation times were most likely due to the different structural organizations induced by the ionic liquids. Photographs of these xerogels are presented in Fig. 2. A translucent and compact monolith was obtained in the presence of methanesulfonate IL **1**. In strong contrast, tetrafluoroborate IL **2** resulted in the formation of a free flowing white powder. Hexafluorophosphate IL **3** induced the formation of silica with porcelain like appearance. Apparently, the IL anion exerts a strong influence on the outcome of these sol–gel reactions.

A scanning electron microscopy study provided insight into the role of the ILs **1–3** as morphology controllers in the formation of the silicas **S1–3**. The SEM micrographs of **S1–3** before extraction of the ILs are presented in Fig. 3. A xerogel with a flat surface was obtained in the presence of methanesulfonate IL **1** (Fig. 3a). Besides, this micrograph shows various layers, which could indicate that **S1** was a lamellar silica xerogel. However, these layers could also be produced due to drying stress by wrinkling. Figure 3b shows that the tetrafluoroborate anion of IL **2** induced the formation of a xerogel with a totally different morphology. In this case, a xerogel (**S2**) that consisted of aggregated spherical particles was obtained. **S3** was prepared in the presence of hexafluorophosphate IL **3** and its micrograph (Fig. 3c) shows that its surface has a high roughness.

The silica xerogels **S1–3** were submitted to a Soxhlet extraction with acetone for 24 h. Thermogravimetric analyses (TGA: Supplementary Material, Fig. S1–3) were performed to determine the IL content before and after extraction of the silica xerogels **S1–3** (Table 1). IL recovery from **S1** was thwarted and resulted in a poor recovery of 15% IL **1**. This was most likely related to the compact nature of **S1** (Fig. 2a), which resulted in a strong confinement of the methanesulfonate IL within the silica network. The high IL content of **S1** after extraction is in agreement with its low specific surface area and low average pore volume (Table 1, entry 1). In contrast, removal of the tetrafluoroborate IL **2** and hexafluorophosphate IL **3** was much more efficient (83% and 97%, respectively), which explains their higher specific surface areas and higher average pore volumes (Table 1, entries 2–3). IL recovery could be an important issue to obtain an economically viable process. ^{1}H NMR analyses did not indicate significant decomposition of the recovered ILs **1**

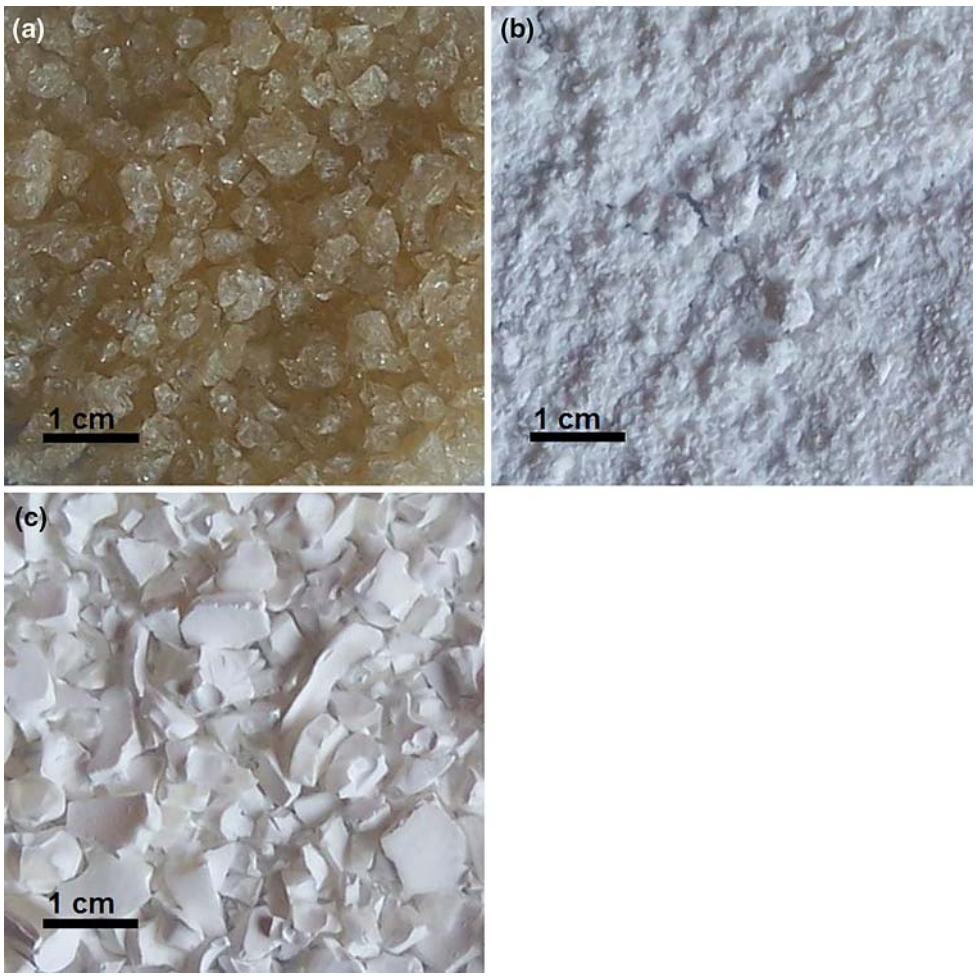

Fig. 2 Photographs of silica xerogels (**a**) **S1** (IL = **1** $[C_3O_1MIm][H_3CSO_3]$); (**b**) **S2** (IL = **2** $[C_3O_1MIm][BF_4]$) and (**c**) **S3** (IL = **3** $[C_3O_1Mim][PF_6]$); before grinding

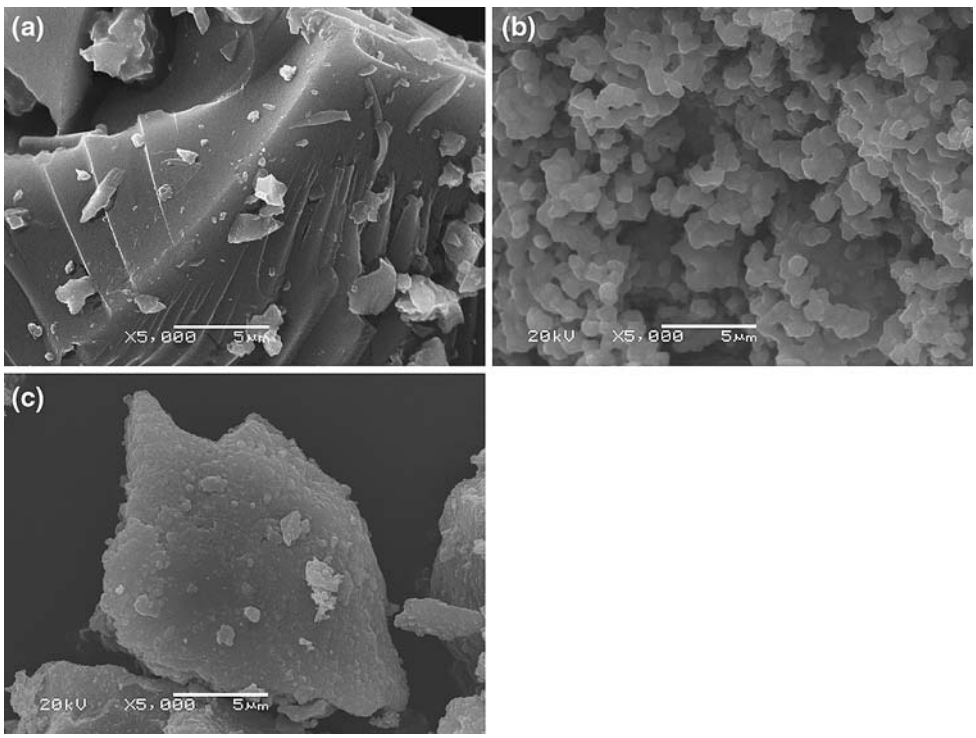

Fig. 3 SEM micrographs of silica xerogels (**a**) **S1** (IL = **1** $[C_3O_1MIm][H_3CSO_3]$); (**b**) **S2** (IL = **2** $[C_3O_1MIm][BF_4]$) and (**c**) **S3** (IL = **3** $[C_3O_1Mim][PF_6]$); before extraction (5,000 magnification, scale bar = 5 μm)

Table 1 Ionic liquid content and textural properties of the xerogels **S1–3**

Entry	Silica	Before extraction % IL	After extraction		
			% IL	S_{BET} ($m^2\ g^{-1}$)[a]	V_p ($cm^3\ g^{-1}$)[b]
1	**S1**	27	23	33	0,02
2	**S2**	40	7	102	0,11
3	**S3**	66	2	97	0,12

[a] S_{BET} = specific surface area determined by BET method

[b] V_p = average pore volume determined by BJH method

and **2**, which suggests the possibility of their reutilization in multiple sol–gel preparations (Supplementary Material, Fig. S4–5). However, hexafluorophosphate IL **3** suffered from serious decomposition after its confinement in xerogel **S3**. The TGA trace of **S3** before extraction shows that IL **3** decomposes at much lower temperatures (160 °C) in comparison to its unsupported form (Supplementary Material, Fig. S3). This is due to the instability of the hexafluorophosphate anion and its tendency to form HF [25].

In general, no pores were visible/detected before extraction. In case of xerogel **S3**, this situation changed dramatically after extraction. Its surface was completely modified and many pores were detected by SEM (Fig. 4). Isolated regions with honeycomb shapes were identified. These shapes appeared at fractured locations, which suggest the presence of many macropores below the compact top layer. The formation of these macropores could be the result of IL microdroplets/spherical organized IL [26]. The honeycomb morphology of **S3** also explains the easy removal of hexafluorophosphate IL **3** by extraction.

Atomic force microscopy after extraction allowed obtaining a more detailed picture of the silica xerogel surfaces (Fig. 5). The roughness values were 49, 894 and

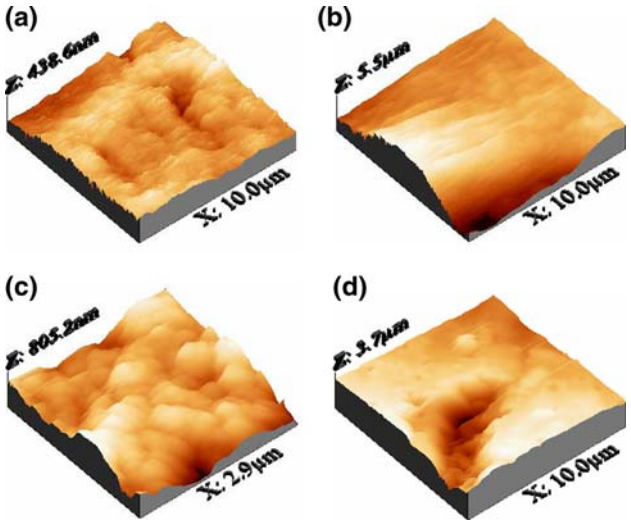

Fig. 5 AFM images of (**a**) **S1** (IL = **1** $[C_3O_1MIm][H_3CSO_3]$); (**b**, **c**) **S2** (IL = **2** $[C_3O_1MIm][BF_4]$) and (**d**) **S3** (IL = **3** $[C_3O_1MIm][PF_6]$); after extraction

521 nm for **S1**, **S2** and **S3**, respectively. These considerable differences and the AFM images are in agreement with the SEM micrographs (Fig. 3). Figure 5a shows the flat surface of **S1**, and its lamellar organization (XZ direction) [27]. The less uniform surface and spherical morphology of **S2** is clearly observed in its AFM images (Fig. 5b, c), which explains the high roughness of this material. Xerogel **S3** presented large surface irregularities, which was due to the hexafluorophosphate IL **3** induced macropores and fractured regions (Fig. 5d).

An XRD study was performed to investigate the structural organization of the silica xerogels **S1–3**. Figure 6 shows the XRD diffractograms of the silica xerogels **S1–3** after extraction. The extracted silicas **S2** and **S3**, synthesized in the presence of ILs with tetrafluoroborate and hexafluorophosphate anions, showed only a broad peak at 23°, which is characteristic for completely amorphous

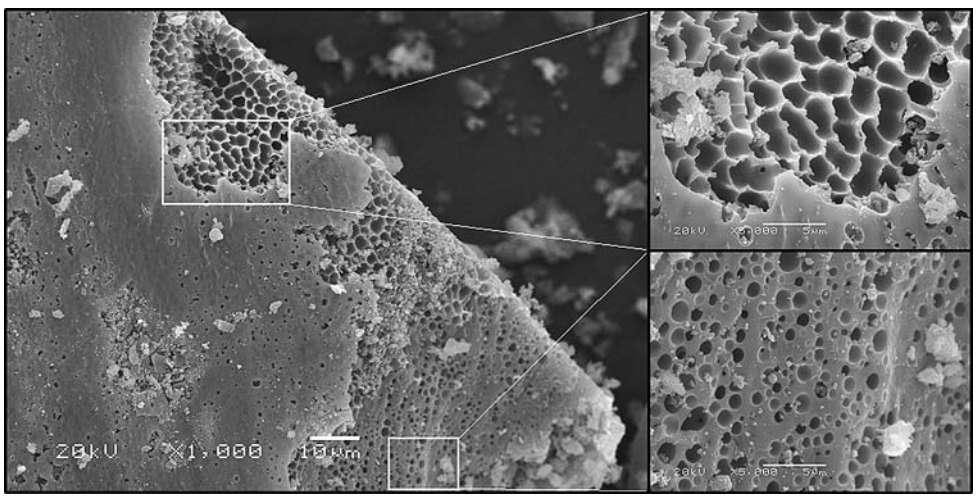

Fig. 4 SEM micrographs of silica xerogel **S3** (IL = **3** $[C_3O_1MIm][PF_6]$) after extraction (1,000 magnification (scale bar = 10 µm) and 5,000 magnification (scale bar = 5 µm))

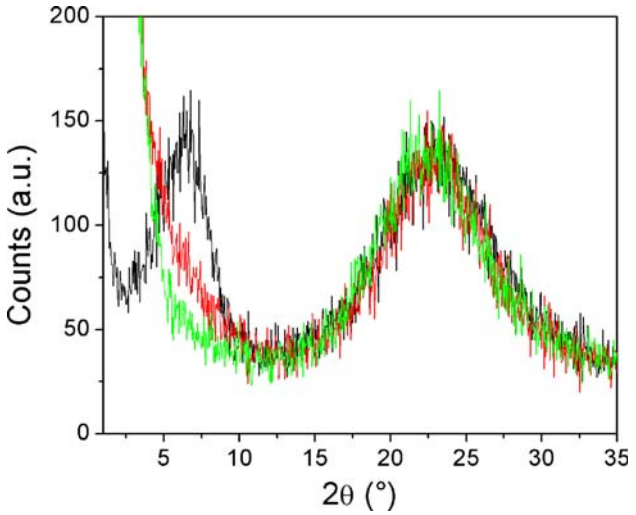

Fig. 6 XRD diffractograms of **S1** (black line, IL = **1** [C_3O_1MIm][H_3CSO_3]); **S2** (red line, IL = **2** [C_3O_1MIm][BF_4]) and **S3** (green line, IL = **3** [C_3O_1MIm][PF_6]); after extraction

materials [28, 29]. In contrast, extracted silica **S1** showed an additional peak at 6°, which could be due to long range periodic ordering of IL **1** that was still present in a high content after extraction. However, there are no significant differences in the XRD diffractograms of the silicas **S1–3** before (Supplementary Material, Fig. S6) and after (Fig. 6) extraction (Supplementary Material, Fig. S7–9). As a consequence, the absence of the additional reflection in the XRD diffractograms of the silicas **S2** and **S3** after extraction was not due to the efficient removal of the ILs **2** and **3** (Table 1). Furthermore, IL **1** itself does not present a reflection in this range (Supplementary Material, Fig. S10). Based on these results it is possible to ascribe the reflection at 6° to the presence of crystalline regions in the silica network of **S1**. This reflection is characteristic for a lamellar silica [30, 31], which provided further evidence for the lamellar nature of xerogel **S1** that was indicated by its SEM micrograph and AFM image. Application of the Bragg equation ($n\,\lambda = 2\,d\,\sin\theta$) allowed to determine the **S1** interlamellar distance of 1.5 nm.

Although speculative, the presented results suggest that the IL anions interact directly with the growing silica networks, which would be in agreement with the previously reported hydrogen bond-*co*-π–π-stack mechanism [13]. A possible reason for the IL anion dependent xerogel morphologies could be the hydrogen bond strength between the anion and the silanol groups of the silica surface. Another explanation could be found in the molecular structure of the IL anions, where the geometry of the anion could induce structural directionality in the forming silica network. The geometry of the methanesulfonate, tetrafluoroborate and hexafluorophosphate anions are square planar, tetrahedral and octahedral, respectively. Furthermore, the number of positions where hydrogen bonding formation could take place is different for each anion. IL solubility in the reaction mixture could be another explanation. The solubility of ILs is strongly affected by the nature of the anion [2, 11], which determines if the ILs are present as solvent separated ions, contact ion pairs, triple ions or supramolecular aggregates. Most likely, hexafluorophosphate IL **3** formed supramolecular aggregates (microdroplets), which induced the formation of the honeycomb structures of **S3**.

4 Conclusions

In summary, the 1-monoethylene glycol monomethyl ether-3-methylimidazolium cation based ILs **1–3** allowed to study the influence of their anions in the sol–gel preparation of silica xerogels. Each IL induced the formation of xerogels with highly distinct structures. The methanesulfonate anion of IL **1** induced the formation of a compact lamellar monolith with a flat surface. A free flowing powder of aggregated spherical particles was obtained in the presence of tetrafluoroborate IL **2**. The hexafluorophosphate anion of IL **3** induced the formation of porcelain like aggregates with honeycomb shapes. This shows that the imidazolium IL anion offers a powerful tool for the preparation of differentiated xerogels, which could furnish access to innovative applications in a wide variety of sciences. A more detailed study about the role of the IL cation and anion in this simple sol–gel procedure is part of our ongoing research.

Acknowledgements The authors thank the CNPq for financial support. M. A. Benvegnú thanks the CNPq for a PIBIC/UFRGS fellowship.

References

1. Wasserscheid P, Welton T (2002) Ionic liquids in synthesis. VCH-Wiley, Weinheim
2. Dupont J, de Souza RF, Suarez PAZ (2002) Chem Rev 102:3667
3. Abraham MH, Zissimos AM, Huddleston JG, Willauer HD, Rogers RD, Acree WE Jr (2003) Ind Eng Chem Res 42:413
4. Pârvulescu VI, Hardacre C (2007) Chem Rev 107:2615
5. Migowski P, Dupont J (2007) Chem Eur J 13:32
6. Ott LS, Finke RG (2007) Coord Chem Rev 251:1075
7. Yang Z, Pan W (2005) Enzyme Microb Technol 37:19
8. de Souza RF, Padilha JC, Gonçalves RS, de Souza MO, Rault-Berthelot J (2007) J Power Sources 164:792
9. Dupont J, Suarez PAZ (2006) Phys Chem Chem Phys 8:2441
10. Consorti CS, Suarez PAZ, de Souza RF, Burrow RA, Farrar DH, Lough AJ, Loh W, da Silva LHM, Dupont J (2005) J Phys Chem B 109:4341
11. Dupont J (2004) J Brazil Chem Soc 15:341
12. Antonietti M, Kuang DB, Smarsly B, Yong Z (2004) Angew Chem Int Edit 43:4988

13. Zhou Y, Schattka JH, Antonietti M (2004) Nano Lett 4:477
14. Taubert A (2005) Acta Chim Slov 52:183
15. Wang T, Kaper H, Antonietti M, Smarsly B (2007) Langmuir 23:1489
16. Karout A, Pierre AC (2007) J. Non-Cryst Sol 353:2900
17. Schrekker HS, Silva DO, Gelesky MA, Stracke MP, Schrekker CML, Gonçalves RS, Dupont J (2008) J Brazil Chem Soc 19:426
18. Donato RK, Migliorini MV, Benvegnú MA, Dupont J, Gonçalves RS, Schrekker HS (2007) J Solid State Electrochem 11:1481
19. Migliorini MV, Donato RK, Benvegnú MA, Dupont J, Gonçalves RS, Schrekker HS (2008) Catal Commun 9:971
20. Schrekker HS, Stracke MP, Schrekker CML, Dupont J (2007) Ind Eng Chem Res 46:7389
21. Schrekker HS, Gelesky MA, Stracke MP, Schrekker CML, Machado G, Teixeira SR, Rubim JC, Dupont J (2007) J Colloid Interface Sci 316:189
22. Branco LC, Rosa JN, Ramos JJM, Afonso CAM (2002) Chem Eur J 8:3671
23. Cassol CC, Ebeling G, Ferrera B, Dupont J (2006) Adv Synth Catal 348:243
24. Gelesky MA, Chiaro SSX, Pavan FA, dos Santos JMZ, Dupont J (2007) Dalton Trans 47:5549
25. Blake DM, Moens L, Rudnicki D, Pilath H (2006) J Sol Energy Eng 128:54
26. Taubert A (2005) Acta Chim Slov 52:168
27. Zhou Y (2005) Curr Nanosci 1:35
28. Wan Y, Yu SH (2008) J Phys Chem C 112:3641
29. Hoffmann HS, Staudt PB, Costa TMH, Moro CC, Benvenutti EV (2002) Surf Interface Anal 33:631
30. Arenas LT, Pinheiro AC, Ferreira JD, Livotto PR, Pereira VP, Gallas MR, Gushikem Y, Costa TMH, Benvenutti EV (2008) J Colloid Interface Sci 318:96
31. Zhou Y, Antonietti M (2003) Adv Mater 15:1452